Radiative Cooling and Improved Confinement in ASDEX Upgrade

A. Kallenbach, R. Dux, A. Bard, S. de Peña Hempel, J. C. Fuchs, A. Gude, H. Salzmann, J. Schweinzer, M. Weinlich and the ASDEX Upgrade Team
MPI für Plasmaphysik, EURATOM Association, D-85748 Garching, Germany

Introduction

The typical experimental domain of radiatively cooled scenarios is characterized by strong gas puffing and cold divertor conditions. While almost complete power removal by radiation could be demonstrated on ASDEX Upgrade with neon cooling [1], only moderate energy confinement improvement above the L-mode level ($H^{ITER89p} \approx 1.6$) is obtained. On the other hand, very good confinement ($H^{ITER89p} > 2$) can be achieved with very low neutral flux levels in the main chamber which is synonymous for a low SOL electron density. In this case, the confinement improvement is attributed to an edge barrier, leading to a pressure pedestal. But, divertor electron temperatures are high for these conditions. In this paper, such a discharge with edge pedestal and neon radiative cooling is compared with the standard cold divertor, type-III ELMy CDH-scenario, where confinement gain is attributed to core density profile peaking. The radiative efficiency $P_z = \delta P_{rad}/\delta Z_{eff}$ turns out to be degraded for the hot divertor conditions. The origin of this degradation is investigated by impurity transport modelling.

Radiative cooling for hot divertor conditions

Fig. 1 shows time traces of a discharge (#8197) with slightly increased triangularity and plasma volume and a low SOL electron density (see Table 1). A short neon puff at t=3 s leads to a moderate increase of the core radiation and a weak reduction of the target power load. The ELM frequency is reduced from 60 Hz to 14 Hz, resulting in high peak target power loads after the neon puff. While the generally lower ELM frequency is attributed to the higher triangularity, it can not be distinguished whether the improved confinement is caused by the plasma shaping directly or by the low neutral flux level / SOL electron density. The long ELM events which can be seen in Fig. 1 after the neon puff consist of short bursts of individual ELMs: The quiescent H* phases are terminated by a type-I ELM which is succeeded by 2-4 type III ELMs within 10 milliseconds. The sawtooth

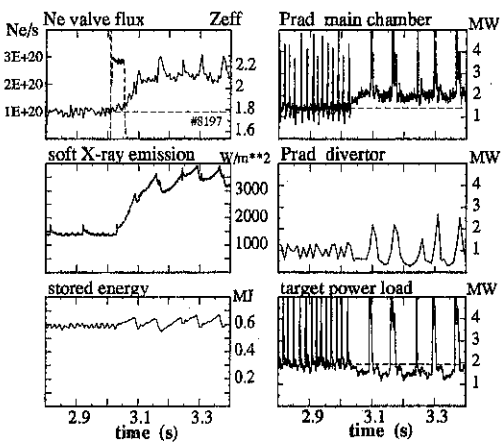

Figure 1: Time traces of a discharge with hot divertor, good energy confinement ($H^{ITER89p} = 2$) and moderate radiative cooling with neon. $P_{heat} = 5$ MW $D^0 \rightarrow D^+$ NBI.

frequency is 14 Hz throughout the discharge, after the neon puff, the sawteeth appear right after the ELM bursts. The improved confinement scenario exhibits a very thin and hot SOL and divertor plasma with an electron temperature $T_e \approx 40$ eV at the outer target.

Radiative efficiency transport modelling

The temporal development of impurity profiles is modelled with the impurity transport code STRAHL [2], using measured electron density and temperature profiles. The STRAHL output interface allows direct comparison with bolometry, spectroscopy, soft-X measurements and charge-exchange recombination spectroscopy (fully stripped impurity density profiles). The overall consistency of STRAHL output and measurements is typically within $\pm$ 30 % when all the diagnostics mentioned are adjusted simultaneously.

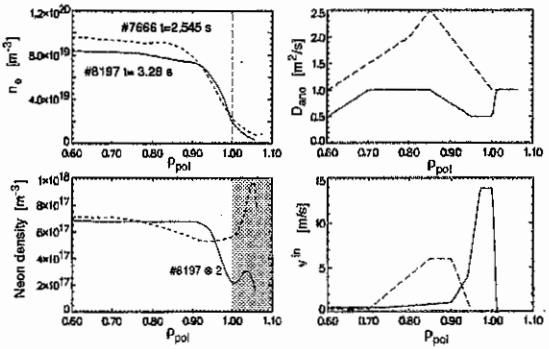

Figure 2: Edge electron and neon density profiles and transport parameters for modelling of the discharge shown in Fig. 1. Parameters of a 'standard' type-III ELMy discharge with moderate gas puffing are given in dotted lines for comparison.

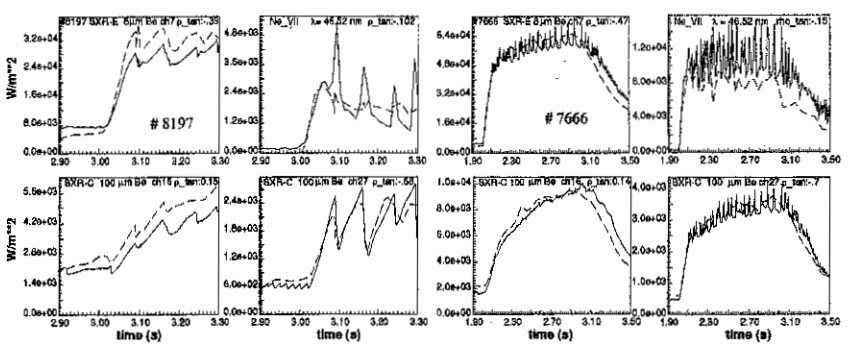

Figure 3: Time traces of soft-X emissivity and Ne^{VII} VUV line emissivity for the discharge shown in Fig. 1 and the reference discharge for comparison. (— model, - - - exp.)

Transport coefficients and density profiles in the outer plasma for the H* phase of Fig. 1 are shown in Fig. 2, values for a standard type-III ELMy discharge with neon cooling are given for comparison. Inside $\rho_{pol} = 0.8$, transport coefficients (D, v) are taken from dynamic pulse analysis using charge exchange recombination spectroscopy [3]. The transport coefficients for $\rho_p > 0.8$ are adapted for different discharge scenarios by matching the temporal evolution of SXR emissivities for various viewing lines and different filter thicknesses (8 and 100 μm Be). While with the 100 μm filters only continuum radiation is measured, with the 8 μm filters also line radiation of highly ionized species contributes.

The radiation profiles before the neon injection are simulated assuming carbon as single impurity (C concentration ≈ 2 %) and matching its influx. After the neon puff, the carbon influx is kept on its initial value, the transport coefficients (D,v) are taken identical to those of neon. The ELMs are simulated by increasing the diffusivity to D= 12 m^2/s over 5 cm inside the separatrix, the radiation during ELMs is not modelled due to the lack of fast enough $T_e(r)$, $n_e(r)$ diagnostics. Sawteeth are treated using an analytical model for the profile reorganization. Experiment and modelling are compared in Fig. 3. It should be noted, that the transport model shown in Fig. 1 represents a possible, but not the unique solution for the observed fluxes and profile shapes if the uncertainties of the measurements are taken into account (see, e.g., [4]). In fact, simultaneously doubling D and v for # 8197 over 3 cm inside the separatrix results in a prediction of the experimental data with a consistency which is similar to the results shown in Fig. 3. Fortunately, the ratio v/D is more robust than the individual values. The question arises, whether the strong neon inward drift during the H* phase is due to neoclassical effects. Fig. 4 shows the various contributions to v_{neo}, the density gradient driven Pfirsch-Schlüter term dominating the ∇T term. In combination with an anomalous D of 1 m^2/s (which is higher than what one would expect within a transport barrier), the neoclassical v_{neo} would fit the experimental data. However, there are uncertainties connected to v_{neo} since the C-Ne collisions and the influence of the radial electric field E_r are not considered in its calculation. Further, an anomalous inward pinch has to be used to reproduce the steep deuteron profile shown in Fig. 2 with simple 1-d modelling including the effect of charge exchange.

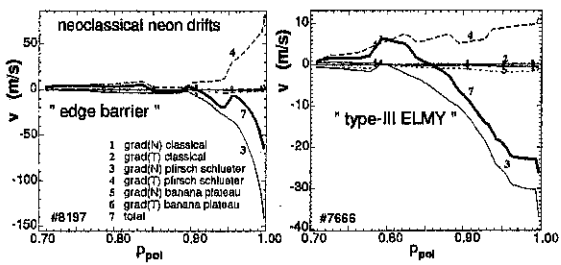

Figure 4: Neoclassical drifts of neon for the discharge shown in Fig. 1, t= 3.28 s and # 7666 for comparison.

We arrive at the following picture of the impurity transport: In the H-mode, D and v peak around ρ_{pol} = 0.8-0.9, and a transport barrier near the separatrix occurs during the H* phases. Between ELMs, anomalous diffusion is reduced within the barrier and a strong inward drift is seen just inside the separatrix. This inward drift leads to a fast impurity build-up close inside the separatrix, its magnitude is similar to the neoclassical level. The clearly anomalous inward drift around ρ_{pol}=0.85 does not lead to substantial impurity buildup since it is compensated by the large values of D. No distinct differences are seen in the radiative efficiencies of radiative type-III ELMy H- and L-modes, where the possible contribution of a neoclassical inward drift is masked by anomalous transport or ELMs.

Origin of the poor radiative efficiency with edge pedestal

The main reason for the poor radiative characteristics of the discharge with edge pedestal is the peaking of the impurity density profile with respect to its edge value. If the transport is characterized by diffusivity D and drift v, the relative profile shape is given by the peaking factor $F_{peak} = exp(-\int_a^r v/Ddr')$. High values of F_{peak} at radial positions with low specific emissivity means plasma pollution without radiative pay-off and

#	type	$H^{ITER89P}$	δ	n_0^{div}; $\overline{n}_e^{SOL}$		T_e^{div}	P_z	$P_z^{\rho<1}$	$F_{peak}^{\rho=0.9}$
				$[10^{19}\ m^{-3}]$		[eV]	[MW]	[MW]	
8197	edge pedestal	2	0.12	1.5	0.6	40	1.8	1.4	4.5
7666	type-III ELMs	1.6	0.09	10	1.0	7	3.5	2	1.1

Table 1: Comparison of radiative characteristics of two improved confinement scenarios with radiative cooling. δ refers to triangularity, T_e^{div} is the peak temperature from target Langmuir probes, P_z is total neon main chamber radiation per core neon Z_{eff} increase. I_p= 1 MA, q_{95}=4.

therefore low values of P_z. The situation for the discharges in comparison is illustrated in Fig. 5: A high drift velocity is only effective to produce profile peaking when connected to a region with low D.

Conclusions

The major drawback for radiative cooling of a discharge with edge pressure pedestal, expressed by the low radiative efficiency $\delta P_{rad}/\delta Z_{eff}$, originates from the large values of v_{in}/D close to the separatrix. Significant values of v_{in} are obtained from neoclassical effects, however, an anomalous contribution to v_{in} may be present. During type-III ELMy or L-mode phases, the neoclassical drifts are masked by other mechanisms and strong profile peaking near the edge is not observed. To obtain efficient radiative cooling, a radiator should be chosen which exhibits its peak emissivity just inside the transport barrier. Other means to increase the radiative efficiency would be density/temperature profile control to support neoclassical drift terms with outward direction. Since the power bursts connected to ELMs succeeding long quiescent H* phases will contradict lifetime requirements of the divertor in a reactor, rapid pellet injection could be used to trigger ELMs with controlled frequency which flatten the impurity profile shape over the pedestal region. The necessary frequency depends on the time scale for buildup of the impurity pedestal and on the width Δ of the pedestal $f \propto v/\Delta$. For designing a reactor scenario with 'edge pedestal', better estimates for the edge transport coefficients, including the neoclassical ones, are required to allow for calculation of the trade-off between confinement degradation and more efficient radiative cooling as well as helium exhaust. To achieve this, refinement of the edge diagnostics is highly desirable.

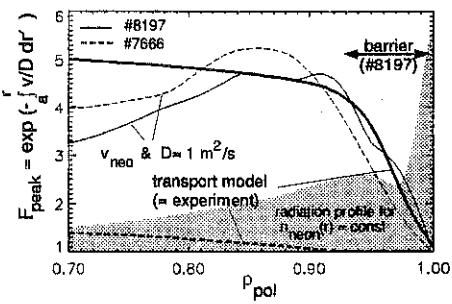

Figure 5: Impurity profile peaking factor F_{peak} for the anomalous transport model of Fig. 2 (fat lines) and for neoclassical drifts according to Fig. 4 and D= 1 m^2/s. The normalized neon radiation profile for #8197 is obtained by multiplication of F_{peak} with the specific emissivity (shaded curve)

References

[1] A. Kallenbach et al., Nucl. Fus. **35** (1995) 1231.
[2] R. Dux et al., PPCF **38** (1996) 989.
[3] S. de Peña Hempel et al., this conference.
[4] R. Giannella et al., Nucl. Fus. **34** (1994) 1185.